Inorganic Chemistry

pubs.acs.org/IC Article

Thermally Robust and Color-Tunable Blue-Green-Emitting $BaMgSi_4O_{10}:Eu^{2+},Mn^{2+}$ Phosphor for Warm-White LEDs

Jiyou Zhong, Ya Zhuo, Shruti Hariyani, Weiren Zhao,* Weidong Zhuang,* and Jakoah Brgoch*

Cite This: *Inorg. Chem.* 2020, 59, 13427−13434 Read Online

ACCESS | Metrics & More | Article Recommendations

ABSTRACT: The dual emission produced from Mn^{2+} when codoped with rare earth ions like Eu^{2+} or Ce^{3+} in inorganic compounds makes these materials attractive as efficient, color-tunable phosphors for warm-white solid-state lighting. Here, a series of efficient blue-green-emitting $BaMgSi_4O_{10}:Eu^{2+},Mn^{2+}$ phosphors with thermally robust, tunable luminescence are reported. Steady-state and time-resolved photoluminescence spectroscopy reveal that Eu^{2+} and Mn^{2+} each occupy a single crystallographic site and confirm that energy transfer occurs from Eu^{2+} to Mn^{2+}. The internal and external quantum efficiency of $BaMgSi_4O_{10}:Eu^{2+},Mn^{2+}$ can reach as high as 69.0 and 47.5%, respectively, upon 360 nm excitation. Moreover, this phosphor possesses nearly zero-thermal quenching up to 440 K due to thermally induced electron detrapping. A fabricated UV-excited white LED device incorporating the blue-green-emitting $BaMgSi_4O_{10}:Eu^{2+},Mn^{2+}$ and the red-emitting $Sr_2Si_5N_8:Eu^{2+}$ phosphors exhibits an excellent CRI of 94.3 with a correlated color temperature of 3967 K. These results prove the potential applications of Eu^{2+},Mn^{2+} codoped $BaMgSi_4O_{10}$ phosphor for generating warm-white light.

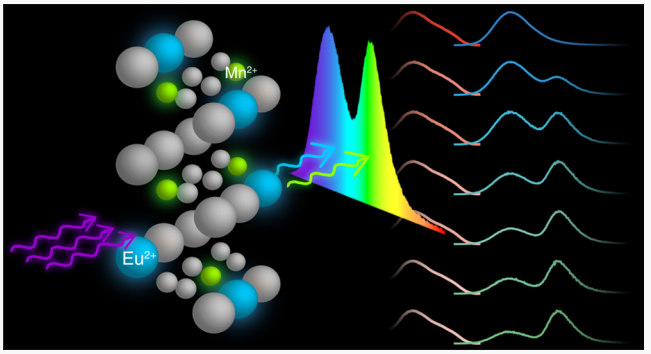

INTRODUCTION

The phosphor-converted white-light-emitting diode (pc-wLED) is an indispensable light source because of its high luminous efficacy, long operating lifetime, and environmentally benign components compared to incandescent and compact fluorescent light bulbs.[1−4] One approach for constructing a pc-wLED is by using a near-UV (360−420 nm) LED chip as the excitation source in combination with three phosphors (red, green, and blue emitting materials).[5−7] This has proven to be an excellent method for achieving a high color rendering index (CRI) and superior color uniformity in a warm-white light.[8,9] However, this technology has high manufacturing costs partly because of the limited number of suitable phosphors available.[10,11] Moreover, fluorescence reabsorption results in low luminous efficiency, and different aging rates of the phosphors cause the pc-wLED's color to change over time.[12,13] It is, therefore, necessary to produce new phosphors to tackle these issues.

The development of new phosphors with strong absorption in the UV region has recently focused on color-tunable materials where the emission covers a wide region of the visible spectrum.[14,15] Co-doping is widely considered one of the most reliable strategies to create color-tunable phosphors.[16−19] Energy transfer between doping ions can significantly promote the luminescent efficiency and color reproducibility as well as widen the emission spectra of phosphors.[12,13,20] Typically, Ce^{3+}-Eu^{2+} and Eu^{2+}/Ce^{3+}-Mn^{2+} energy transfer are adopted to produce a broad blue-green or blue-red emission.[21−23] Unfortunately, the emission color of these phosphors usually shifts as a function of temperature and shows a commensurate decrease in efficiency.[24,25] This is likely because the two luminescent centers have different thermal quenching properties. In particular, Mn^{2+} often suffers from severe thermal quenching.[26−28] Thus, developing optically tunable phosphors with not only a highly efficient emission but also thermally robust luminescence is a significant challenge.

$BaMgSi_4O_{10}$ was first reported by Toropov et al. to crystallize in the tetragonal space group *P*4/*ncc* and be isostructural with the mineral gillespite, shown in Figure 1a.[29] The basic structural units in this original report include a $[SiO_4]$ tetrahedron, a $[BaO_8]$ dodecahedron, and a peculiar $[MgO_4]$ square planar unit. However, the simulated X-ray diffraction pattern created using this structure model (shown in red in Figure 1b), does not completely match their

Received: June 18, 2020
Published: September 1, 2020

https://dx.doi.org/10.1021/acs.inorgchem.0c01803
Inorg. Chem. 2020, 59, 13427−13434

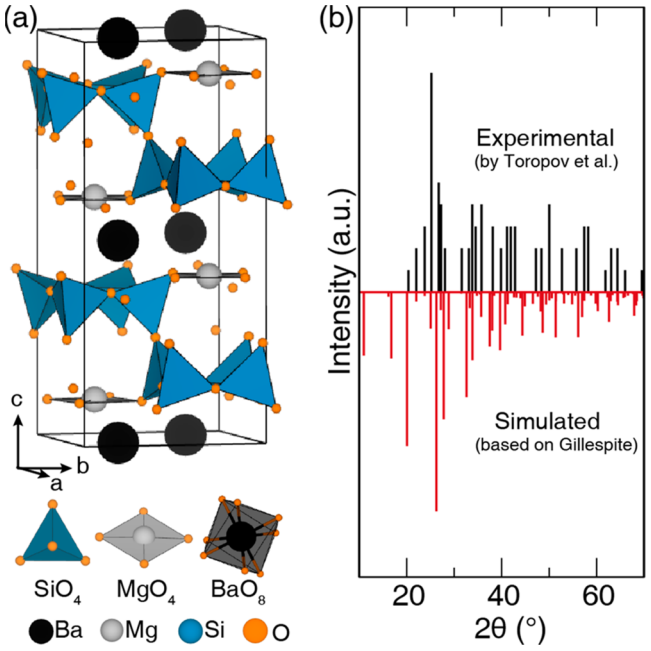

Figure 1. (a) Crystal structure of $BaMgSi_4O_{10}$ with the proposed gillespite structure; (b) original reported experimental powder X-ray diffractogram of $BaMgSi_4O_{10}$ compared with a simulated diffractogram of the gillespite structure taken from the International Centre for Diffraction Data (ICDD) database.

experimental data (shown as the black data in Figure 1b). A similar conclusion is drawn in a brief study of $BaMgSi_4O_{10}:Eu^{2+}$ as an inorganic phosphor,[30] implying the wrong structure and incomplete experimental data for $BaMgSi_4O_{10}$ have been recorded in the database and that more work is needed to reveal the exact crystal structure of this compound. Nevertheless, the $BaMgSi_4O_{10}:Eu^{2+}$ phosphor was reported to have an intense blue emission (centered at ~465 nm) and good thermal stability under ultraviolet excitation.[30,31] However, a majority of the essential optical properties, such as particle morphology and quantum efficiency (QE) were not reported for this phosphor. Of greater interest is the fact that the Mg^{2+} site in the structure makes it suitable for Mn^{2+} doping because of their similarity in ionic size. Generally, Mn^{2+} presents a linear absorption in the ultraviolet to blue region due to the spin-forbidden $^4T_1$-$^6A_1$ transition and exhibits green emission in a four-coordinated environment or red emission in a six-coordinated environment.[32] As a result, codoping Eu^{2+},Mn^{2+} in $BaMgSi_4O_{10}$ should produce an energy transfer from Eu^{2+} to Mn^{2+} that is expected to result in a color-tunable phosphor.

In this work, we performed a systematic investigation of the $BaMgSi_4O_{10}:Eu^{2+},Mn^{2+}$ codoped phosphor to understand the optical properties and potential for color-tunable photoluminescence, including identifying the energy transfer and thermal quenching mechanisms. The $BaMgSi_4O_{10}:Eu^{2+},Mn^{2+}$ phosphor exhibits a blue-green color-tunable character with nearly zero-thermal-quenching property for both the Eu^{2+} and Mn^{2+} emission centers, while maintaining a high quantum efficiency. Combining $BaMgSi_4O_{10}:Eu^{2+},Mn^{2+}$ blue-green-emitting phosphor and $Sr_2Si_5N_8:Eu^{2+}$ red-emitting phosphor with a 370 nm LED chip produced a white-LED device with a high color rendering index (*Ra*) of 94.3 and a low correlated color temperature (CCT) of 3967 K, indicating the potential applications of this phosphor in near-UV-pumped warm white-LEDs.

EXPERIMENTAL METHODS

Synthesis. $(Ba_{1-x}Eu_x)(Mg_{1-y}Mn_y)Si_4O_{10}$ (x = 0, 0.04; y = 0, 0.02, 0.04, 0.06, 0.08, 0.1, and 0.12) was prepared by conventional high-temperature solid-state reaction using $BaCO_3$ (Aldrich, 99.99%), $4MgCO_3{\cdot}Mg(OH)_2{\cdot}5H_2O$ (Aldrich, 99.9%), SiO_2 (Aldrich, 99.95%), $MnCO_3$ (Aldrich, 99.99%), and Eu_2O_3 (Aldrich, 99.995%) as the starting materials. The starting materials were first weighed out according to the required stoichiometric ratio, and then mixed thoroughly using a shaker mill (Spex 8000M) in a polystyrene vial with two methacrylate balls (Φ = 9.5 mm) as grinding media for 30 min. The homogeneous mixtures were subsequently placed in a graphite crucible and heated at 1353 K for 12 h under a reducing atmosphere (5% H_2/95% N_2) using a heating and cooling rate of 3 K/min. The final product was ground into a fine powder using an agate mortar and pestle.

Characterization. X-ray diffractograms were collected on an X'Pert3 PANalytical (Cu Kα, λ = 1.5406 Å) equipped with an Anton-Paar TTK450 temperature chamber. The scanning electron micrographs (SEM) and energy-dispersive spectroscopy (EDS) maps were collected on a Hitachi-S4800 (Japan). The room-temperature and temperature-dependent photoluminescent spectra were recorded using a PTI QuantaMaster with a 75 W xenon arc lamp for excitation and a Janis cryostat (VPF-100) to control the temperature between 80 and 500 K. The time-gated photoluminescence decay measurements of Eu^{2+}-doped samples were collected using a Horiba DeltaFlex Lifetime System. The decay curves of Mn^{2+}-doped samples were collected using an FLS-980 fluorescence spectrophotometer (Edinburgh Instruments) equipped with a xenon flash lamp (450 W, Osram) as the excitation source. The internal and external quantum efficiency (QE) were measured using the integrating sphere on the QE-2100 quantum yield measurement system (Otsuka Electronics Co., Ltd., Japan), and a Xe lamp as the excitation source with $BaSO_4$ powder as a reference. The thermoluminescence (TL) curves were collected by a thermoluminescence meter (SL08-L, Guangzhou-Radiation Science and Technology Co. Ltd.) with the heating rate of 1 K/s after being excited for 5 min under 254 nm lamp. The diffuse reflection (DR) spectra were detected on a UV−vis−NIR spectrophotometer (SHIMADZU, Japan) with an integrated sphere attachment and $BaSO_4$ powder as a standard. The pc-LED device was fabricated by using a 370 nm LED combined with a phosphor "cap", which was prepared by curing an intimate mixture of $Ba_{0.96}Eu_{0.04}Mg_{0.96}Mn_{0.04}Si_4O_{10}$, lab-made $Sr_2Si_5N_8:Eu^{2+}$, and a transparent silicone resin (GE Silicones, RTV615) in a custom brass mold. The electroluminescence spectrum, CRI, and CCT of the pc-LED device were measured under a forward bias of 20 mA using an AvaFast fiber optic Vis/NIR spectrometer coupled to a 50 mm integrating sphere.

RESULTS AND DISCUSSION

Synthesis, Phase, and Morphology. The synthesis of $BaMgSi_4O_{10}$ (BMSO) was first reported by Toropov et al.,[29] where the crystalline product was prepared from the prolonged crystallization of a $BaMgO_2[SiO_2]_4$ glass at 1223 K. Analyzing the standard card (PDF no. 15−0182) in crystal structure databases and comparing these data to the experimental X-ray diffractogram suggests an incomplete crystal structure solution. Despite this, Inoue et al.,[30] synthesized an Eu^{2+}-substituted $BaMgSi_4O_{10}$ ($BMSO:Eu^{2+}$) phosphor by sintering the powder twice at 1373 K. These samples showed an intense diffraction peak near $2\theta \approx 30°$, which was ascribed to the product, but it is not in the original report by Toropov et al. Yuan et al.,[31] also synthesized $BMSO:Eu^{2+}$ and this sample matched the original standard card. Their synthesis involved a two-step reaction of sintering at 1273 and 1473 K. Considering the significant

https://dx.doi.org/10.1021/acs.inorgchem.0c01803
Inorg. Chem. 2020, 59, 13427−13434

differences in crystal structure stemming from the sintering temperatures in previous work, here, we systematically investigated the relationship between phase formation and reaction temperature. The optimized sintering temperature to prepare a phase-pure sample was found to be 1353 K. This route produced single-phase $BaMgSi_4O_{10}$ identical to the sample presented by Inoue et al. Interestingly, sintering above 1373 K causes the samples to melt, and sintering below 1343 K results in $BaSi_2O_5$ impurity. The product prepared at 1353 K can be confidently claimed to be single phase. This is because numerous adjustments to the reaction conditions including temperature, adding flux, multistep sintering, and pressing a pellet of the raw powder before heating resulted in a powder pattern that contained the diffraction peak near 30°. More importantly, the relative intensity of peaks never changed in all of these samples. Thus, this corroborates the work by Inoue et al., where the diffraction peak near 30° indeed belongs to BMSO.

BMSO:Eu^{2+} and the Mn^{2+}-substituted $BaMgSi_4O_{10}$ (BMSO:Mn^{2+}) phosphors were subsequently synthesized at 1353 K. Additionally, a series of $Ba_{1-x}Eu_xMg_{1-y}Mn_ySi_4O_{10}$ (BMSO:Eu^{2+},Mn^{2+}) were also produced. The X-ray diffraction patterns of these samples (presented as Figure 2) show

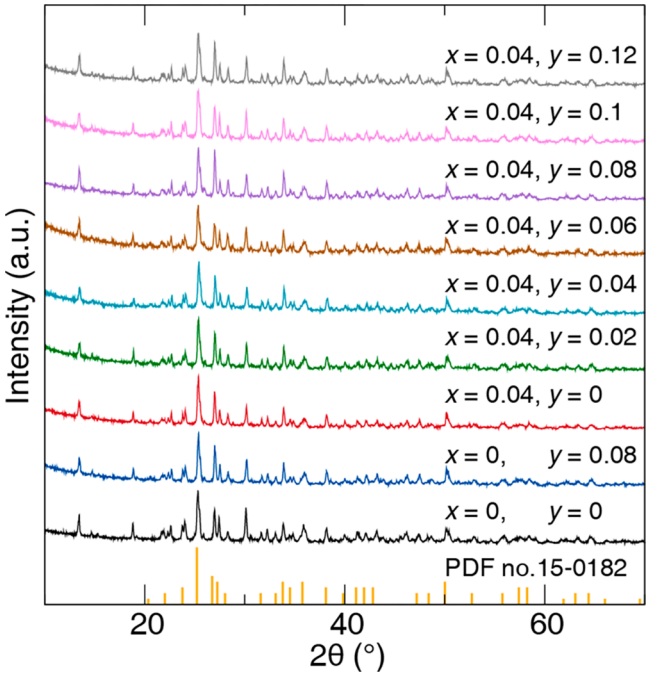

Figure 2. X-ray diffraction patterns of $Ba_{1-x}Eu_xMg_{1-y}Mn_ySi_4O_{10}$ (x = 0 or 0.04, y = 0–0.12) compared with standard card (PDF no. 15–0182) for $BaMgSi_4O_{10}$.

excellent agreement with the compounds reported by Inoue et al.[30] No other phases could be indexed, indicating that no impurities and structural variations occur upon doping. Unfortunately, solving the structure from powder X-ray diffraction is nearly impossible because of the random orientation of the crystals. The most reliable way to determine the crystal structure is through single-crystal diffraction. The particle size of these samples is only tens of micrometers, which is too small to obtain a dependable single-crystal pattern. Thus, an exact structure solution remains elusive, and additional work is needed to grow larger single crystals to solve this compound's structural uncertainty.

Analyzing the morphology of synthesized $Ba_{0.96}Eu_{0.04}Mg_{0.96}Mn_{0.04}Si_4O_{10}$ sample using SEM (Figure 3a)

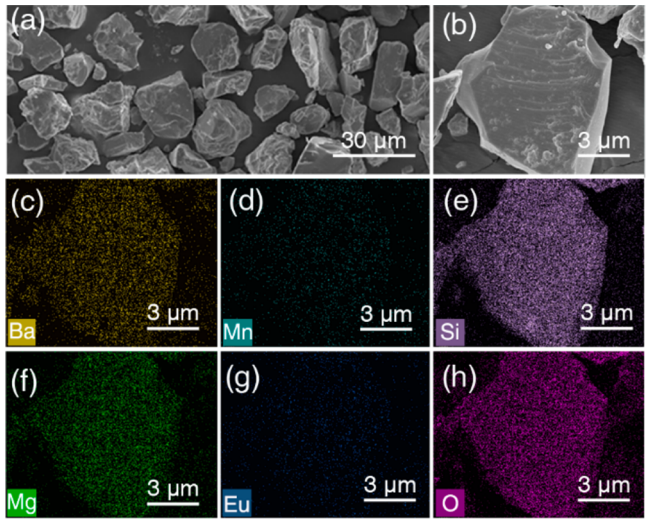

Figure 3. (a) Scanning electron microscopy (SEM); (b–h) energy-dispersive spectrum (EDS) mapping on single particle of sample $Ba_{0.96}Eu_{0.04}Mg_{0.96}Mn_{0.04}Si_4O_{10}$.

shows that all of the particles are irregular in shape with a size of 10–20 μm. EDS mapping (shown in Figure 3b–h) indicates that the elements Ba, Mg, Si, Eu, and Mn contained in this sample are homogeneously distributed within a single particle.

Diffuse Reflection Spectra and Photoluminescence Properties. The diffuse reflection spectra of BMSO, BMSO:Eu^{2+}, and BMSO:Eu^{2+},Mn^{2+} were examined (Figure 4a–c). BMSO:Eu^{2+} and BMSO:Eu^{2+},Mn^{2+} both present an

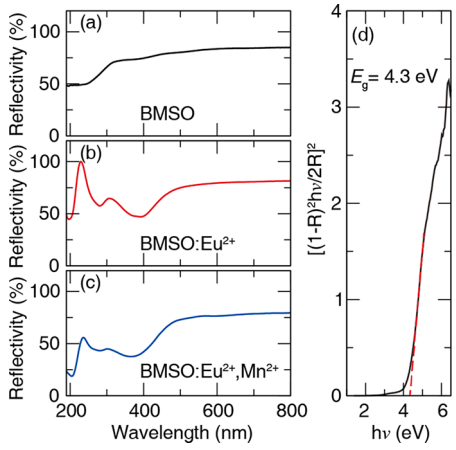

Figure 4. Diffuse reflectance spectra of (a) $BaMgSi_4O_{10}$ host, (b) $Ba_{0.96}MgSi_4O_{10}$:0.04Eu^{2+} phosphor, and (c) $Ba_{0.96}Mg_{0.96}Si_4O_{10}$:0.04$Eu^{2+}$,0.04$Mn^{2+}$ phosphor; (d) optical band gap calculation of host.

intense absorption in the UV and near-UV region (250–420 nm), which can be ascribed to the $4f^7 \rightarrow 4f^65d^1$ transitions of the Eu^{2+} ions. The absorption cutoff edge of the host is ~288 nm, and the optical band gap (E_g) can be estimated to be 4.3 eV based on the data plotted in Figure 4d.

https://dx.doi.org/10.1021/acs.inorgchem.0c01803
Inorg. Chem. 2020, 59, 13427–13434

The photoluminescent excitation and emission of BMSO:Eu^{2+} were measured and are plotted in Figure 5a.

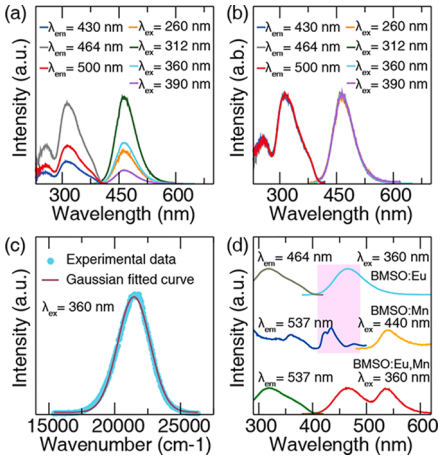

Figure 5. (a) Photoluminescent excitation spectra monitored at different emission wavelengths (λ_{em} = 430−500 nm) and emission spectra with different excitations (λ_{ex} = 260−390 nm) of BMSO: 0.04Eu^{2+} sample; (b) the corresponding normalized excitation and emission spectra; (c) Gaussian fitting emission spectrum of BMSO: 0.04Eu^{2+} excited by 360 nm; (d) room-temperature excitation and emission spectra of BMSO: 0.04Eu^{2+}, BMSO: 0.08Mn^{2+} and BMSO: 0.04Eu^{2+}, 0.04Mn^{2+} phosphor.

These data show that this phosphor exhibits a blue emission with the peak centered at 464 nm upon UV excitation. The excitation spectrum (λ_{em} = 464 nm) covers a broad range spanning from 250 to 400 nm, following previous reports.[30,31] Noticeably, the normalized emission spectra (Figure 5b) with different excitations varying from 260 to 390 nm overlap, indicating a large possibility of single emission center in this sample and further supports a structure solution with a single crystallographic Ba^{2+} site in BMSO. Additionally, the normalized excitation spectra of BMSO:Eu^{2+} monitored at different emission wavelengths ranging from 430 to 500 nm also nearly overlap, further confirming that the broad emission of Eu^{2+} in BMSO is derived from different vibrational levels of a single emission center.[33] Moreover, the emission spectrum excited by 360 nm can be well fitted by a single Gaussian band (shown in Figure 5c), which is direct evidence for Eu^{2+} substituting a single crystallographic Ba^{2+} site in BMSO.

Analyzing the Mn^{2+}-doped $BaMgSi_4O_{10}$ (BMSO:Mn^{2+}) sample presents a weak yellow-green emission peak centered at 537 nm (Figure 5d), suggesting Mn^{2+} occupies a four-coordinated Mg^{2+} site. Considering the considerable overlap between the excitation band of BMSO:Mn^{2+} and the emission band of BMSO:Eu^{2+}, an effective resonance energy transfer in the BMSO:Eu^{2+},Mn^{2+} phosphor is expected. Fixing the Eu^{2+} concentration at x = 0.04 and then gradually increasing the Mn^{2+} concentration (y = 0.02−0.12) causes the emission contribution from Eu^{2+} at 464 nm to decrease, whereas the emission intensity of Mn^{2+} at 537 nm increases (Figure 6). This occurs until the concentration quenching limit at y = 0.1. As a result, this series of phosphors exhibit intense, tunable emission from blue to yellow-green as a function of Mn^{2+} concentration (illustrated as inset of Figure 6). Interestingly, the normalized excitation spectra of the Eu^{2+}-doped sample (λ_{em} = 464 nm) and the Eu^{2+}-Mn^{2+} codoped samples (λ_{em} = 537 nm) show no difference, indicating most of the emission

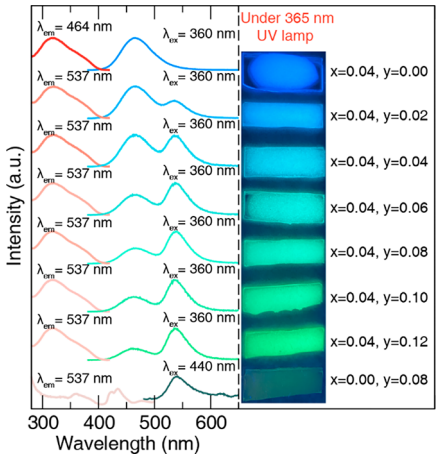

Figure 6. Room-temperature excitation (λ_{em} = 537 or 464 nm) and emission (λ_{ex} = 360 or 440 nm) spectra of $Ba_{1-x}Eu_xMg_{1-y}Mn_ySi_4O_{10}$ (x = 0 or 0.04; y = 0−0.12); inset is the corresponding digital photos of phosphor-coated slides under 365 nm UV lamp.

energies of Mn^{2+} originates from Eu^{2+} absorption followed by energy transfer.

Energy Transfer Mechanism. Time-gated photoluminescence decay curves were collected (plotted in Figure 7) to

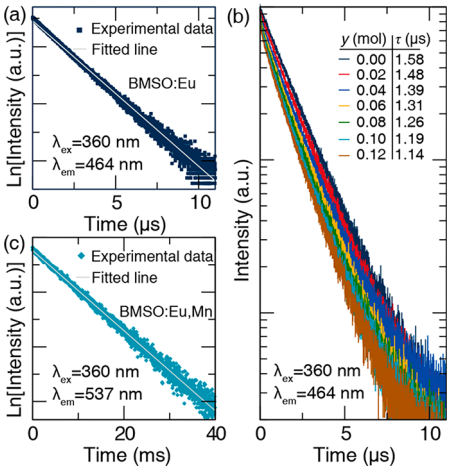

Figure 7. (a) Linear fitting of ln(I) vs t in $Ba_{0.96}Eu_{0.04}MgSi_4O_{10}$; (b) PL decay curves of Eu^{2+} (λ_{ex} = 360 nm, λ_{em} = 464 nm) in $Ba_{1-x}Eu_xMg_{1-y}Mn_ySi_4O_{10}$ (x = 0.04; y = 0−0.12) samples; and (c) PL decay curve of Mn^{2+} (λ_{ex} = 360 nm, λ_{em} = 537 nm) in $Ba_{0.96}Eu_{0.04}Mg_{0.96}Mn_{0.04}Si_4O_{10}$.

investigate the energy transfer process. The decay curve of Eu^{2+} in $BaMgSi_4O_{10}$ can be fit to a single exponential function (shown as Figure 7a), supporting the idea that only one Eu^{2+} emission center is present in the crystal structure. However, the decay curves of Eu^{2+} in $Ba_{1-x}Eu_xMg_{1-y}Mn_ySi_4O_{10}$ (x = 0.04; y = 0.02−0.12) samples (presented in Figure 7b) slightly deviate from the single exponential function, and the lifetime decreases gradually from 1.48 to 1.14 μs with increasing y, due to the energy transfer from Eu^{2+} to Mn^{2+}. The decay curve of Mn^{2+} (depicted as Figure 7c) in the Eu^{2+}-Mn^{2+} codoped phosphor system also exhibits a single exponential character, indicating only one type of Mg^{2+} site available for Mn^{2+}.

The energy transfer efficiency, η_T, from Eu^{2+} to Mn^{2+} can be calculated based on the lifetimes of Eu^{2+} with the following equation[34]

https://dx.doi.org/10.1021/acs.inorgchem.0c01803
Inorg. Chem. 2020, 59, 13427−13434

$$\eta_T = 1 - \tau_S/\tau_{S0} \quad (1)$$

where τ_{S0} and τ_S represent the lifetimes of Eu^{2+} with the absence and the presence of Mn^{2+}, respectively. The energy transfer efficiency, η_T, as a function of Mn^{2+} doping concentration is given in Figure 8a. As shown, η_T gradually

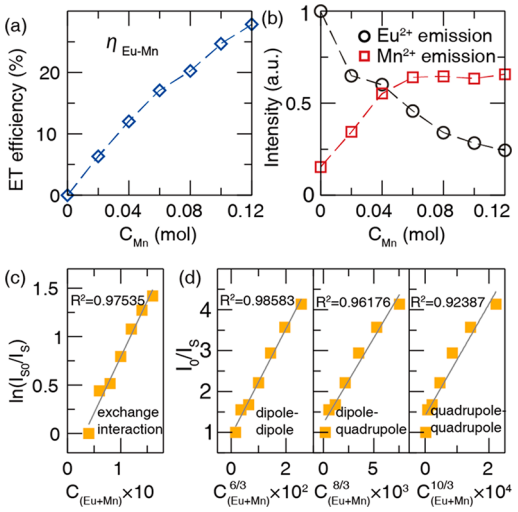

Figure 8. (a) Energy transfer efficiency η_T as a function of Mn^{2+} doping concentration; (b) emission intensities of Eu^{2+} and Mn^{2+} under 360 nm excitation; (c) relationship between $\ln(I_{S0}/I_S)$ of Eu^{2+} and C; (d) dependence of I_{S0}/I_S of Eu^{2+} on $C^{6/3}$, $C^{8/3}$, and $C^{10/3}$ in $Ba_{1-x}Eu_xMg_{1-y}Mn_ySi_4O_{10}$ (x = 0.04; y = 0−0.12) samples.

increases with increasing Mn^{2+} concentration and reaches an efficiency of ∼30% with 12 mol % Mn^{2+} doping concentration. This relatively low value of η_T implies that a small part of the energy absorbed by Eu^{2+} ions is assigned to Mn^{2+}. A similar situation can also be found in Ce^{3+}-Mn^{2+} codoped γ-AlON phosphor.[35] The η_T is possible to be further increased by increasing Mn^{2+} doping concentration, but the increasing concentration quenching of Mn^{2+} may result in low emission efficiency as well.

Generally, the energy transfer mechanisms are exchange interactions and electric multipolar interactions. According to Dexter's energy transfer theory and Reisfeld's approximation, the interactions can be determined by the following equations[36−39]

$$\ln\frac{\eta_0}{\eta_s} \propto C_{Eu^{2+}+Mn^{2+}} \text{ and } \frac{\eta_0}{\eta_s} \propto C^{n/3}_{Eu^{2+}+Mn^{2+}} \quad (2)$$

where η_0 and η_s are the luminescence quantum efficiencies of Eu^{2+} in the absence and presence of Mn^{2+}, respectively. The values of η_0/η_s can be estimated approximately by the ratio of relative luminescence intensity ratio (I_{S0}/I_S) (shown as Figure 8b) and C is the sum of the concentrations of Eu^{2+} and Mn^{2+}. Finally, a proportional relationship between $\ln(I_{S0}/I_S)$ and $C(Eu^{2+}+Mn^{2+})$ corresponds to exchange interaction, whereas the relationship I_{S0}/I_S versus $C^{n/3}$ ($Eu^{2+}+Mn^{2+}$) with n = 6, 8, and 10 correspond to dipole−dipole (d−d), dipole−quadrupole (d−q), and quadrupole−quadrupole (q−q) interactions, respectively.[40] The relationships between I_{S0}/I_S and $C^{n/3}$ ($Eu^{2+}+Mn^{2+}$) are depicted in Figure 8c, d. As presented, the best linear behavior evaluated through comparing the fitting factor, R^2, is observed only when n = 6, implying that energy transfer from Eu^{2+} to Mn^{2+} occurs via the dipole−dipole mechanism.

Temperature-Dependent Photoluminescence. Thermal stability is a key criterion that should be evaluated for any practical phosphor application.[41,42] The emission spectra of the $BaMgSi_4O_{10}$:0.04Eu^{2+} and $BaMgSi_4O_{10}$:0.04Eu^{2+},0.04Mn^{2+} phosphors excited by 360 nm near-ultraviolet light were investigated from 80 to 520 K. As shown in Figure 9, the

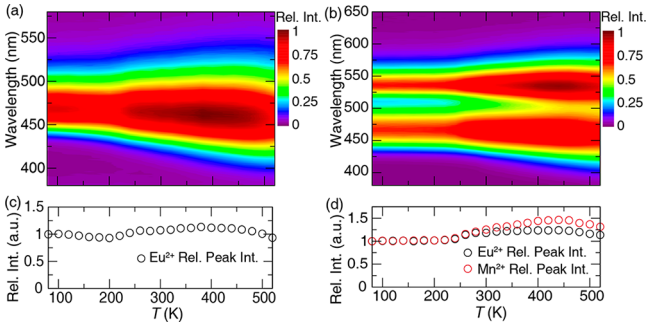

Figure 9. Contour plot of the emission spectra of (a) $BaMgSi_4O_{10}$:0.04Eu^{2+}, and (b) $BaMgSi_4O_{10}$:0.04Eu^{2+},0.04Mn^{2+} phosphor excited at 360 nm as a function of temperature. The normalized intensity of the emission peak (norm. peak int.) of (c) $BaMgSi_4O_{10}$:0.04Eu^{2+} and (d) $BaMgSi_4O_{10}$:0.04Eu^{2+},0.04Mn^{2+} phosphors as a function of temperature.

relative emission intensity of $BaMgSi_4O_{10}$:0.04Eu^{2+} is found to decrease slightly with increasing temperature reaching a minimum at 200 K, followed by an increase, reaching the maximum at 260 K. The emission is then stable until 440 K and finally decreases with further heating. Fortunately, there is minimal thermal quenching in the temperature range from 300 to 440 K, which is usually the operating temperature for LED devices, making this phosphor viable for application in LED-based light bulbs. Also, the Eu^{2+} in $BaMgSi_4O_{10}$:0.04Eu^{2+},0.04Mn^{2+} phosphor possesses an outstanding thermal performance, similar to that in the $BaMgSi_4O_{10}$:0.04Eu^{2+} phosphor. However, the Mn^{2+} presents the same trend in emission intensity but has a surprisingly better thermal performance than the Eu^{2+} in $BaMgSi_4O_{10}$:0.04Eu^{2+},0.04Mn^{2+} phosphor. This indicates that the energy transfer efficiency (η_T) is not changed as the temperature varies and that the Mn^{2+} luminescence in this codoped phosphor has high thermal stability, which is rare. Moreover, the emission peak from Mn^{2+} broadens without a shift in emission wavelength, whereas the Eu^{2+} emission also broadens with a gradual blue-shift (∼10 nm) in the measured temperature range.

Two traditional models can explain thermal quenching process, i.e., crossing relaxation and thermal ionization.[43,44] Crossing relaxation can be characterized by the activation energy for thermal quenching, E_a, which is experimentally obtained by fitting the temperature-dependent emission data to the Arrhenius equation. Thermal ionization can be characterized by E_{dc}, the energy difference between the highest 5d level and the bottom of the conduction band, which usually occurs in phosphor systems with a narrow band gap.[41,45] However, our experimental thermal quenching measurements inferred that both of these models could not be applied to this phosphor system because of the complex variations of emission intensity as a function of temperature. Recently, a defect-related model was proposed to interpret the increase in

https://dx.doi.org/10.1021/acs.inorgchem.0c01803
Inorg. Chem. 2020, 59, 13427−13434

emission intensity with increasing temperature.[42,46] This model states that electrons detrapping from defect states can compensate for the emission intensity loss caused by thermal quenching. The zero-thermal quenching property in phosphors such as $Na_3Sc_2(PO_4)_3$:Eu^{2+} and $K_2BaCa(PO_4)_2$:Eu^{2+}[42,47] can be explained with this model. To support the existence of defects in our phosphor, we collected the thermoluminescence (TL) spectra of $BaMgSi_4O_{10}$:$0.04Eu^{2+}$ and $BaMgSi_4O_{10}$:$0.04Eu^{2+}$,$0.04Mn^{2+}$ in the temperature range of 300−780 K after being excited with 254 nm ultraviolet light for 5 min (Figure 10). As presented, the TL curve of $BaMgSi_4O_{10}$:$0.04Eu^{2+}$ shows a wide distribution that can be well fitted with three Gaussian bands centered at 351, 409, and 520 K, corresponding to trap depths of 0.70, 0.82, and 1.04 eV, respectively. These values are estimates obtained from the rough relationship $E_T = T/500$ eV, where T is the temperature in kelvin (K).[48] Moreover, the trap depths in the Eu^{2+}-Mn^{2+} codoped sample are the same as Eu^{2+} doped sample, but the concentration of each kind of defect is different. To fully understand the mechanism of thermally induced electron detrapping, a complete structure solution for this phosphor is still necessary, which will be the goal of our future work.

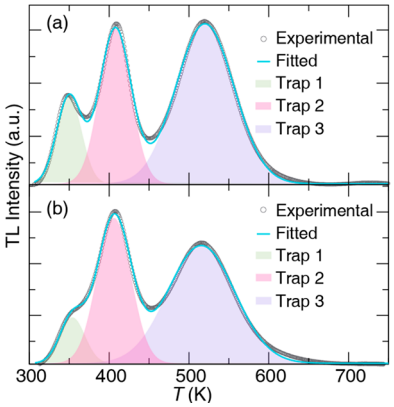

Figure 10. TL curves and Gaussian deconvolutions of (a) $BaMgSi_4O_{10}$:$0.04Eu^{2+}$, and (b) $BaMgSi_4O_{10}$:$0.04Eu^{2+}$,$0.04Mn^{2+}$ phosphor collected in the temperature range of 300−780 K.

Quantum Efficiency and CIE Coordinates. A previous report indicated BMSO:Eu^{2+} has high emission efficiency under 310 nm excitation, being comparable with that of YAG:Ce^{3+} excited by 460 nm;[30] however, the quantum efficiency under near-UV excitation remains unknown. To further evaluate the practical use of this phosphor, we measured the internal and external quantum efficiency (IQE, EQE) and CIE coordinates of $Ba_{1-x}Eu_xMg_{1-y}Mn_ySi_4O_{10}$ (x = 0 or 0.04; y = 0−0.12) upon 360 nm excitation and presented them in Figure 11a, b. The IQE and EQE of $BaMgSi_4O_{10}$:$0.04Eu^{2+}$ was determined to be 75.3 and 51.7%, respectively, whereas in the Eu^{2+}-Mn^{2+} codoped $BaMgSi_4O_{10}$ system, the IQE and EQE first increases and then decreases with increasing Mn^{2+} concentration and reaches a maximum of 69.0 and 47.5%, respectively, when $x = y = 0.04$. For comparison, the IQE and EQE values of the commercial blue phosphor BAM:Eu^{2+} was measured to be 92 and 71%, respectively, under 360 nm excitation. Thus, further synthetic optimization is still necessary to promote the QE. The CIE chromaticity coordinates of this phosphor system can be tuned from blue (0.162, 0.168) to yellow-green (0.341, 0.610) shown in Figure 11c, and demonstrates that this phosphor system has a highly tunable emission with a sufficient quantum efficiency.

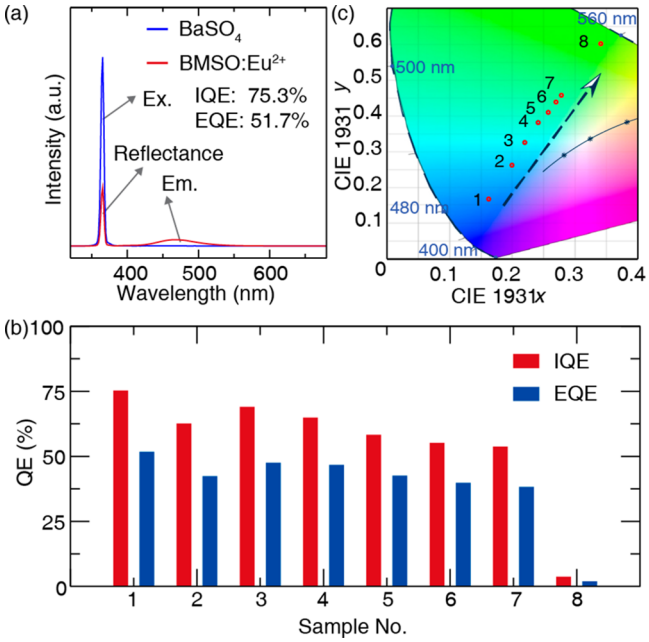

Figure 11. (a) QE measurement of BMSO:Eu^{2+} phosphor; (b) IQE and EQE of $Ba_{1-x}Eu_xMg_{1-y}Mn_ySi_4O_{10}$ (x = 0.04, y = 0−0.12 named no. 1−7; x = 0, y = 0.08 named no. 8); and (c) the corresponding CIE chromaticity coordinates.

Application in Near-UV pc-wLEDs. To evaluate the device performance of the Eu^{2+}-Mn^{2+} codoped $BaMgSi_4O_{10}$ phosphor, we fabricated a pc-wLED using $BaMgSi_4O_{10}$:$0.04Eu^{2+}$,$0.04Mn^{2+}$ as the blue-green-emitting phosphor, $Sr_2Si_5N_8$:Eu^{2+} as the red-emitting phosphor, and a 370 nm NUV chip as the excitation source. This combination of phosphors and LED chip, shown in Figure 12a, generates a warm white light with CIE coordinate of (0.384, 0.383) driven by a 20 mA current (Figure 12b) giving it an acceptable color correlated temperature (CCT = 3967 K) and a high corresponding color rendering index (Ra = 94.3). These results indicate that the Eu^{2+}-Mn^{2+} codoped $BaMgSi_4O_{10}$ phosphor is an efficient blue-green-emitting phosphor and

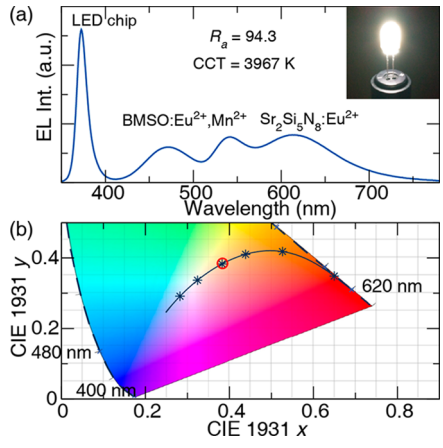

Figure 12. (a) Emission spectrum of a white LED fabricated by $BaMgSi_4O_{10}$:$0.04Eu^{2+}$,$0.04Mn^{2+}$, $Sr_2Si_5N_8$:Eu^{2+}, and a 370 nm LED chip; the inset is the photograph of the white LED under a forward bias of 20 mA. (b) CIE coordinates of the fabricated white LED.

https://dx.doi.org/10.1021/acs.inorgchem.0c01803
Inorg. Chem. 2020, 59, 13427−13434

may be combined with other red phosphors to achieve high-quality UV-excited warm-white pc-LEDs.

CONCLUSIONS

In summary, a series of Eu^{2+}-Mn^{2+} codoped $BaMgSi_4O_{10}$ phosphors were synthesized by conventional high-temperature solid-state reactions. Steady-state and time-resolved photoluminescence spectroscopy indicate that energy transfer occurs from Eu^{2+} to Mn^{2+} through dipole−dipole interactions. Upon 360 nm excitation, the internal and external quantum efficiency of the codoped phosphor reached 69.0 and 47.5%, respectively, and the phosphor shows negligible thermal quenching up to 500 K. The origin of the impressive temperature-dependent properties can be ascribed to thermally released electrons trapped by defects to the 5d Eu^{2+} orbitals. Finally, a NUV-excited (λ_{ex} = 370 nm) pc-wLED device with a CCT = 3967 K and *Ra* = 94.3 was fabricated by combining the blue-green-emitting $BaMgSi_4O_{10}$:0.04Eu^{2+},0.04Mn^{2+} phosphor with red-emitting $Sr_2Si_5N_8$:Eu^{2+}, demonstrating the potential applications of Eu^{2+}-Mn^{2+} codoped $BaMgSi_4O_{10}$ phosphor in pc-wLEDs.

AUTHOR INFORMATION

Corresponding Authors

Weiren Zhao − *School of Physics and Optoelectronic Engineering, Guangdong University of Technology, Guangzhou 510006, China*; Email: zwren123@126.com

Jakoah Brgoch − *Department of Chemistry, University of Houston, Houston, Texas 77204, United States*; orcid.org/0000-0002-1406-1352; Email: jbrgoch@uh.edu

Weidong Zhuang − *National Engineering Research Center for Rare Earth Materials, General Research Institute for Nonferrous Metals, Beijing 100088, China*; Email: wdzhuang@126.com

Authors

Jiyou Zhong − *School of Physics and Optoelectronic Engineering, Guangdong University of Technology, Guangzhou 510006, China*; orcid.org/0000-0003-2817-6617

Ya Zhuo − *Department of Chemistry, University of Houston, Houston, Texas 77204, United States*; orcid.org/0000-0003-2554-498X

Shruti Hariyani − *Department of Chemistry, University of Houston, Houston, Texas 77204, United States*

Complete contact information is available at: https://pubs.acs.org/10.1021/acs.inorgchem.0c01803

Notes

The authors declare no competing financial interest.

ACKNOWLEDGMENTS

The authors thank the National Natural Science Foundation of China (51702057), the National Science Foundation (DMR 18-47701 and CER 19-11311), and the University of Houston Division of Research and the Grant to Enhance and Advance Research for funding this research.

REFERENCES

(1) Schubert, E. F.; Kim, J. K. Solid-State Light Sources Getting Smart. *Science* **2005**, *308* (5726), 1274−1278.

(2) Pimputkar, S.; Speck, J. S.; Denbaars, S. P.; Nakamura, S. Prospects for LED Lighting. *Nat. Photonics* **2009**, *3* (4), 180−182.

(3) Pattison, P. M.; Tsao, J. Y.; Brainard, G. C.; Bugbee, B. LEDs for Photons, Physiology and Food. *Nature* **2018**, *563* (7732), 493−500.

(4) Yao, Q.; Hu, P.; Sun, P.; Liu, M.; Dong, R.; Chao, K.; Liu, Y.; Jiang, J.; Jiang, H. YAG:Ce3+ Transparent Ceramic Phosphors Brighten the Next-Generation Laser-Driven Lighting. *Adv. Mater.* **2020**, *32* (19), 1907888.

(5) Wang, L.; Xie, R. J.; Suehiro, T.; Takeda, T.; Hirosaki, N. Down-Conversion Nitride Materials for Solid State Lighting: Recent Advances and Perspectives. *Chem. Rev.* **2018**, *118* (4), 1951−2009.

(6) Lin, C. C.; Liu, R. S. Advances in Phosphors for Light-Emitting Diodes. *J. Phys. Chem. Lett.* **2011**, *2* (11), 1268−1277.

(7) Liu, Y.; Zhang, J.; Zhang, C.; Xu, J.; Liu, G.; Jiang, J.; Jiang, H. Ba9Lu2Si6O24: CE3+: An Efficient Green Phosphor with High Thermal and Radiation Stability for Solid-State Lighting. *Adv. Opt. Mater.* **2015**, *3* (8), 1096−1101.

(8) Li, G.; Tian, Y.; Zhao, Y.; Lin, J. Recent Progress in Luminescence Tuning of Ce3+ and Eu2+-Activated Phosphors for Pc-WLEDs. *Chem. Soc. Rev.* **2015**, *44* (23), 8688−8713.

(9) Qin, X.; Liu, X.; Huang, W.; Bettinelli, M.; Liu, X. Lanthanide-Activated Phosphors Based on 4f-5d Optical Transitions: Theoretical and Experimental Aspects. *Chem. Rev.* **2017**, *117* (5), 4488−4527.

(10) Sun, L.; Devakumar, B.; Liang, J.; Wang, S.; Sun, Q.; Huang, X. Highly Efficient Ce3+ → Tb3+ Energy Transfer Induced Bright Narrowband Green Emissions from Garnet-Type Ca2YZr2(AlO4)-3:Ce3+,Tb3+ Phosphors for White LEDs with High Color Rendering Index. *J. Mater. Chem. C* **2019**, *7* (34), 10471−10480.

(11) Zhong, J.; Zhuo, Y.; Hariyani, S.; Zhao, W.; Wen, J.; Brgoch, J. Closing the Cyan Gap Toward Full-Spectrum LED Lighting with NaMgBO3:Ce3+. *Chem. Mater.* **2020**, *32* (2), 882−888.

(12) Chen, M.; Xia, Z.; Molokeev, M. S.; Liu, Q. Insights into Ba4Si6O16 Structure and Photoluminescence Tuning of Ba4Si6O16:-Ce3+,Eu2+ Phosphors. *J. Mater. Chem. C* **2015**, *3* (48), 12477−12483.

(13) Guo, C.; Yu, J.; Ding, X.; Li, M.; Ren, Z.; Bai, J. A Dual-Emission Phosphor LiCaBO3:Ce3+,Mn2+ with Energy Transfer for Near-UV LEDs. *J. Electrochem. Soc.* **2011**, *158* (2), J42.

(14) Zhou, J.; Xia, Z. Multi-Color Emission Evolution and Energy Transfer Behavior of La 3GaGe5O16:Tb3+,Eu3+ Phosphors. *J. Mater. Chem. C* **2014**, *2* (34), 6978−6984.

(15) Zhang, X.; Zhu, Z.; Guo, Z.; Sun, Z.; Yang, Z.; Zhang, T.; Zhang, J.; Wu, Z. C.; Wang, Z. Dopant Preferential Site Occupation and High Efficiency White Emission in K2BaCa(PO4)2:Eu2+,Mn2+ Phosphors for High Quality White LED Applications. *Inorg. Chem. Front.* **2019**, *6* (5), 1289−1298.

(16) Huang, D.; Dang, P.; Lian, H.; Zeng, Q.; Lin, J. Luminescence and Energy-Transfer Properties in Bi3+/Mn4+-Codoped Ba2GdN-bO6 Double-Perovskite Phosphors for White-Light-Emitting Diodes. *Inorg. Chem.* **2019**, *58* (22), 15507−15519.

(17) Saavedra-Rodriguez, G.; Pal, U.; Sánchez-Zeferino, R.; Álvarez-Ramos, M. E. Tunable White-Light Emission of Co 2+ and Mn 2+ Co-Doped ZnS Nanoparticles by Energy Transfer between Dopant Ions. *J. Phys. Chem. C* **2020**, *124* (6), 3857−3866.

(18) Dong, L.; Zhang, L.; Jia, Y.; Shao, B.; Lü, W.; Zhao, S.; You, H. Site Occupation and Luminescence of Novel Orange-Red Ca3M2-Ge3O12:Mn2+,Mn4+ (M = Al, Ga) Phosphors. *ACS Sustainable Chem. Eng.* **2020**, *8*, 3357.

(19) An, Z.; Liu, W.; Song, Y.; Zhang, X.; Dong, R.; Zhou, X.; Zheng, K.; Sheng, Y.; Shi, Z.; Zou, H. Color-Tunable Eu2+,Eu3+ Co-Doped Ca20Al26Mg3Si3O68 Phosphor for W-LEDs. *J. Mater. Chem. C* **2019**, *7* (23), 6978−6985.

(20) Li, K.; Shang, M.; Lian, H.; Lin, J. Recent Development in Phosphors with Different Emitting Colors: Via Energy Transfer. *J. Mater. Chem. C* **2016**, *4* (24), 5507−5530.

(21) Zhang, Z.; Ma, C.; Gautier, R.; Molokeev, M. S.; Liu, Q.; Xia, Z. Structural Confinement toward Giant Enhancement of Red Emission in Mn2+-Based Phosphors. *Adv. Funct. Mater.* **2018**, *28* (41), 1804150.

(22) Ha, J.; Kim, Y. H.; Novitskaya, E.; Wang, Z.; Sanchez, M.; Graeve, O. A.; Ong, S. P.; Im, W. B.; McKittrick, J. Color Tunable Single-Phase Eu2+ and Ce3+ Co-Activated Sr2LiAlO4 Phosphors. *J. Mater. Chem. C* **2019**, *7* (25), 7734−7744.

(23) Yan, J.; Zhang, Z.; Wen, D.; Zhou, J.; Xu, Y.; Li, J.; Ma, C. G.; Shi, J.; Wu, M. Crystal Structure and Photoluminescence Tuning of Novel Single-Phase Ca8ZnLu(PO4)7:Eu2+,Mn2+ Phosphors for near-UV Converted White Light-Emitting Diodes. *J. Mater. Chem. C* **2019**, *7* (27), 8374−8382.
(24) Zhang, X.; Xu, J.; Guo, Z.; Gong, M. Luminescence and Energy Transfer of Dual-Emitting Solid Solution Phosphors (Ca,Sr)10Li-(PO4)7:Ce3+,Mn2+ for Ratiometric Temperature Sensing. *Ind. Eng. Chem. Res.* **2017**, *56* (4), 890−898.
(25) Zhang, X.; Zhu, Z.; Guo, Z.; Sun, Z.; Chen, Y. A Ratiometric Optical Thermometer with High Sensitivity and Superior Signal Discriminability Based on Na3Sc2P3O12: Eu2+, Mn2+ Thermochromic Phosphor. *Chem. Eng. J.* **2019**, *356*, 413−422.
(26) Long, Z.; Wen, Y.; Qiu, J.; Wang, J.; Zhou, D.; Zhu, C.; Lai, J.; Xu, X.; Yu, X.; Wang, Q. Crystal Structure Insight Aided Design of SrGa2Si2O8:Mn2+ with Multi-Band and Thermally Stable Emission for High-Power LED Applications. *Chem. Eng. J.* **2019**, *375* (April), 122016.
(27) Xu, Z.; Xia, Z.; Lei, B.; Liu, Q. Full Color Control and White Emission from CaZnOS:Ce3+,Na+,Mn2+ Phosphors: Via Energy Transfer. *J. Mater. Chem. C* **2016**, *4* (41), 9711−9716.
(28) Shi, R.; Ning, L.; Wang, Z.; Chen, J.; Sham, T. K.; Huang, Y.; Qi, Z.; Li, C.; Tang, Q.; Liang, H. Zero-Thermal Quenching of Mn2+ Red Luminescence via Efficient Energy Transfer from Eu2+ in BaMgP2O7. *Adv. Opt. Mater.* **2019**, *7* (23), 1901187.
(29) Toropov, N. A. Barium Dimetasilicates with Layer Structures: MgBaSi4O10 and Ba2Si4O10. *Russ. J. Inorg. Chem.* **1962**, *7* (2), 172−177.
(30) Inoue, M.; Uematsu, K.; Ishigaki, T.; Toda, K.; Sato, M. Synthesis of Gillespite Related Silicate Phosphor for a White LED. In *Meeting Abstracts*; The Electrochemical Society, 2009; pp 3221−3221.
(31) Yuan, B.; Huang, Y.; Yu, Y. M.; Kim, S. I.; Seo, H. J. A New Blue-Emitting Phosphor of Eu 2 + -Doped BaMgSi 4O 10. *Mater. Lett.* **2012**, *70*, 57−59.
(32) Zhou, Q.; Dolgov, L.; Srivastava, A. M.; Zhou, L.; Wang, Z.; Shi, J.; Dramićanin, M. D.; Brik, M. G.; Wu, M. Mn2+ and Mn4+ Red Phosphors: Synthesis, Luminescence and Applications in WLEDs. A Review. *J. Mater. Chem. C* **2018**, *6* (11), 2652−2671.
(33) Chen, L.; Fei, M.; Zhang, Z.; Jiang, Y.; Chen, S.; Dong, Y.; Sun, Z.; Zhao, Z.; Fu, Y.; He, J.; Li, C.; Jiang, Z. Understanding the Local and Electronic Structures toward Enhanced Thermal Stable Luminescence of CaAlSiN3:Eu2+. *Chem. Mater.* **2016**, *28* (15), 5505−5515.
(34) Paulose, P. I.; Jose, G.; Thomas, V.; Unnikrishnan, N. V.; Warrier, M. K. R. Sensitized Fluorescence of Ce3+/Mn2+ System in Phosphate Glass. *J. Phys. Chem. Solids* **2003**, *64* (5), 841−846.
(35) Si, J.; Wang, L.; Liu, L.; Yi, W.; Cai, G.; Takeda, T.; Funahashi, S.; Hirosaki, N.; Xie, R. J. Structure, Luminescence and Energy Transfer in Ce3+ and Mn2+ Codoped γ-AlON Phosphors. *J. Mater. Chem. C* **2019**, *7* (3), 733−742.
(36) Dexter, D. L. A Theory of Sensitized Luminescence in Solids. *J. Chem. Phys.* **1953**, *21* (5), 836−850.
(37) Lahoz, F.; Martín, I. R.; Méndez-Ramos, J.; Núñez, P. Dopant Distribution in a Tm3+-Yb3+ Codoped Silica Based Glass Ceramic: An Infrared-Laser Induced Upconversion Study. *J. Chem. Phys.* **2004**, *120* (13), 6180−6190.
(38) Huang, C. H.; Chen, T. M. A Novel Single-Composition Trichromatic White-Light Ca3Y(GaO) 3(BO3)4:Ce3+,Mn2+,Tb 3+ Phosphor for UV-Light Emitting Diodes. *J. Phys. Chem. C* **2011**, *115* (5), 2349−2355.
(39) Xia, Z.; Liu, R. S. Tunable Blue-Green Color Emission and Energy Transfer of Ca 2Al 3O 6F:Ce 3+,Tb 3+ Phosphors for near-UV White LEDs. *J. Phys. Chem. C* **2012**, *116* (29), 15604−15609.
(40) Jia, Y.; Qiao, H.; Zheng, Y.; Guo, N.; You, H. Synthesis and Photoluminescence Properties of Ce 3+ and Eu 2+-Activated Ca 7Mg(SiO 4) 4 Phosphors for Solid State Lighting. *Phys. Chem. Chem. Phys.* **2012**, *14* (10), 3537−3542.
(41) Zhong, J.; Zhao, W.; Du, F.; Wen, J.; Zhuang, W.; Liu, R.; Duan, C. K.; Wang, L.; Lin, K. Identifying the Emission Centers and Probing the Mechanism for Highly Efficient and Thermally Stable Luminescence in the La3Si6N11:Ce3+ Phosphor. *J. Phys. Chem. C* **2018**, *122* (14), 7849−7858.
(42) Kim, Y. H.; Arunkumar, P.; Kim, B. Y.; Unithrattil, S.; Kim, E.; Moon, S.-H.; Hyun, J. Y.; Kim, K. H.; Lee, D.; et al. Zero-Thermal-Quenching Phosphor. *Nat. Mater.* **2017**, *16* (5), 543−550.
(43) Liu, Y.; Silver, J.; Xie, R. J.; Zhang, J.; Xu, H.; Shao, H.; Jiang, J.; Jiang, H. An Excellent Cyan-Emitting Orthosilicate Phosphor for NUV-Pumped White LED Application. *J. Mater. Chem. C* **2017**, *5* (47), 12365−12377.
(44) Zhong, J.; Zhuang, W.; Xing, X.; Liu, R.; Li, Y.; Liu, Y.; Hu, Y. Synthesis, Crystal Structures, and Photoluminescence Properties of Ce3+-Doped Ca2LaZr2Ga3O12: New Garnet Green-Emitting Phosphors for White Leds. *J. Phys. Chem. C* **2015**, *119* (10), 5562−5569.
(45) Brgoch, J.; Denbaars, S. P.; Seshadri, R. Proxies from Ab Initio Calculations for Screening Efficient Ce3+ Phosphor Hosts. *J. Phys. Chem. C* **2013**, *117* (35), 17955−17959.
(46) Zhang, M.; Xia, Z.; Liu, Q. Thermally Stable KxCs1-xAlSi2O6:Eu2+ Phosphors and Their Photoluminescence Tuning. *J. Mater. Chem. C* **2017**, *5* (30), 7489−7494.
(47) Qiao, J.; Ning, L.; Molokeev, M. S.; Chuang, Y. C.; Liu, Q.; Xia, Z. Eu2+ Site Preferences in the Mixed Cation K2BaCa(PO4)2 and Thermally Stable Luminescence. *J. Am. Chem. Soc.* **2018**, *140* (30), 9730−9736.
(48) Van den Eeckhout, K.; Smet, P. F.; Poelman, D. Persistent Luminescence in Eu2+-Doped Compounds: A Review. *Materials* **2010**, *3* (4), 2536−2566.

https://dx.doi.org/10.1021/acs.inorgchem.0c01803
Inorg. Chem. 2020, 59, 13427−13434